Acta Crystallographica Section D
Biological Crystallography
ISSN 0907-4449

Interactions of a new α-aminophosphinic derivative inside the active site of TLN (thermolysin): a model for zinc-metalloendopeptidase inhibition

Mohamed Selkti,[a]* Alain Tomas,[a] Jean-François Gaucher,[a] Thierry Prangé,[a,b] Marie-Claude Fournié-Zaluski,[c] Huixiong Chen[c] and Bernard-Pierre Roques[c]

[a]Laboratoire de Cristallographie et RMN Biologiques (UMR 8015 CNRS), 4 Avenue de l'Observatoire, 75270 Paris CEDEX 06, France, [b]LURE, Bâtiment 209d, Université Paris-Sud, 91405 Orsay CEDEX, France, and [c]Département de Pharmacochimie Moléculaire et Structurale (INSERM U266–CNRS FRE 2463), 4 Avenue de l'Observatoire, 75270 Paris CEDEX 06, France

Correspondence e-mail: selkti@pharmacie.univ-paris5.fr

Received 13 February 2003
Accepted 7 May 2003

PDB Reference: thermolysin–α-aminophosphinic compound complex, 1os0, r1os0sf.

A new α-aminophosphinic compound able to inhibit both zinc-containing exopeptidases and endopeptidases has been crystallized with TLN as a model in order to investigate the mode of zinc recognition by the phosphinic moiety and to evaluate the potential role of the free α-amino group in the formation of enzyme–inhibitor complexes. In addition to the main interactions between the backbone of the inhibitor and the enzyme active site, it is observed that the phosphinic group acts as a distorted bidentate ligand for the zinc ion, while the free α-amino function does not directly participate in interactions within the active site. Association of the present data and the K_i values of various analogues of the inhibitor towards TLN and neprilysin suggests differences in the hydrophobicity of the S_1–S_2 domains of the enzymes. This could be taken into account in the design of selective inhibitors.

1. Introduction

Thermolysin (TLN; EC 3.4.24.28), a thermostable bacterial protease isolated from *Bacillus thermoproteolyticus*, is considered to be the prototype of zinc metalloproteases belonging to the gluzincin family (MA clan). Indeed, crystallographic analysis of a number of TLN–inhibitor complexes (Matthews, 1988) has allowed an understanding of the mode of binding of these inhibitors and allowed the mechanism of action of these peptidases to be determined (Hangauer *et al.*, 1984; Matthews, 1988). In addition, these mechanistic and structural parameters were extended to other related zinc metallopeptidases, such as the angiotensin-converting enzyme (ACE; EC 3.4.15.1; Bohacek *et al.*, 1996), the endothelin-converting enzyme (ECE; Sansom *et al.*, 1998) and neprilysin (NEP; EC 3.4.24.11; Tiraboschi *et al.*, 1999), the three-dimensional structures of which were unknown at the time. The validity of this approach has recently been confirmed by X-ray analyses of neprilysin (Oefner *et al.*, 2000), human leucotriene A_4 hydrolase (LTA_4H; Thunnissen *et al.*, 2001) and angiotensin-converting enzyme (Natesh *et al.*, 2003). These analyses demonstrated that the three-dimensional structures of the active sites are quite similar to that of TLN. Additional crystallographic studies of other zinc metallopeptidases belonging to other families, such as matrix metallopeptidases (Bode *et al.*, 1993) and botulinum neurotoxins (Swaminathan & Eswaramoorthy, 2000; Hanson & Stevens, 2000), have also shown that most of the structural characteristics of the TLN catalytic site are preserved in these enzymes.

Since the discovery that phosphoramidon (Umezawa *et al.*, 1972) is able to competitively interact with TLN ($K_i = 2.8 \times 10^{-8}$ *M*; Komiyama *et al.*, 1975), a number of phosphorus-

containing peptide analogues have been developed as potent zinc-metallopeptidase inhibitors (Kam *et al.*, 1979; Bartlett & Marlowe, 1983, 1987). Owing to the presence of a tetrahedral P atom in these compounds, it has been suggested that phosphonates, phosphonamidates or phosphinates could mimic the transition state of peptide-substrate hydrolysis. To confirm this hypothesis, a number of phosphonates and phosphonamidates were co-crystallized with TLN (Weaver *et al.*, 1977; Tronrud *et al.*, 1986, 1987; Holden *et al.*, 1987). In all cases it was observed that at least one oxygen of the phosphoryl group binds directly to the Zn^{2+}, while the second oxygen remains in the vicinity of the catalytic glutamate Glu143. Furthermore, both monodentation and bidentation of the zinc ion by O atom(s) of the phosphoryl moiety are observed, depending on the inhibitor structure. Thus, (i) in the TLN–phosphoramidon complex only one oxygen binds Zn^{2+}, leading to tetracoordination (Weaver *et al.*, 1977), (ii) in the complex with $ZF^{P}LA$ (Holden *et al.*, 1987), Zn^{2+} is pentacoordinated owing to bidentation by the two phosphonamide O atoms and (iii) with the small molecule P-Leu-NH_2 (Tronrud *et al.*, 1986) the structure is intermediate between these two modes of binding.

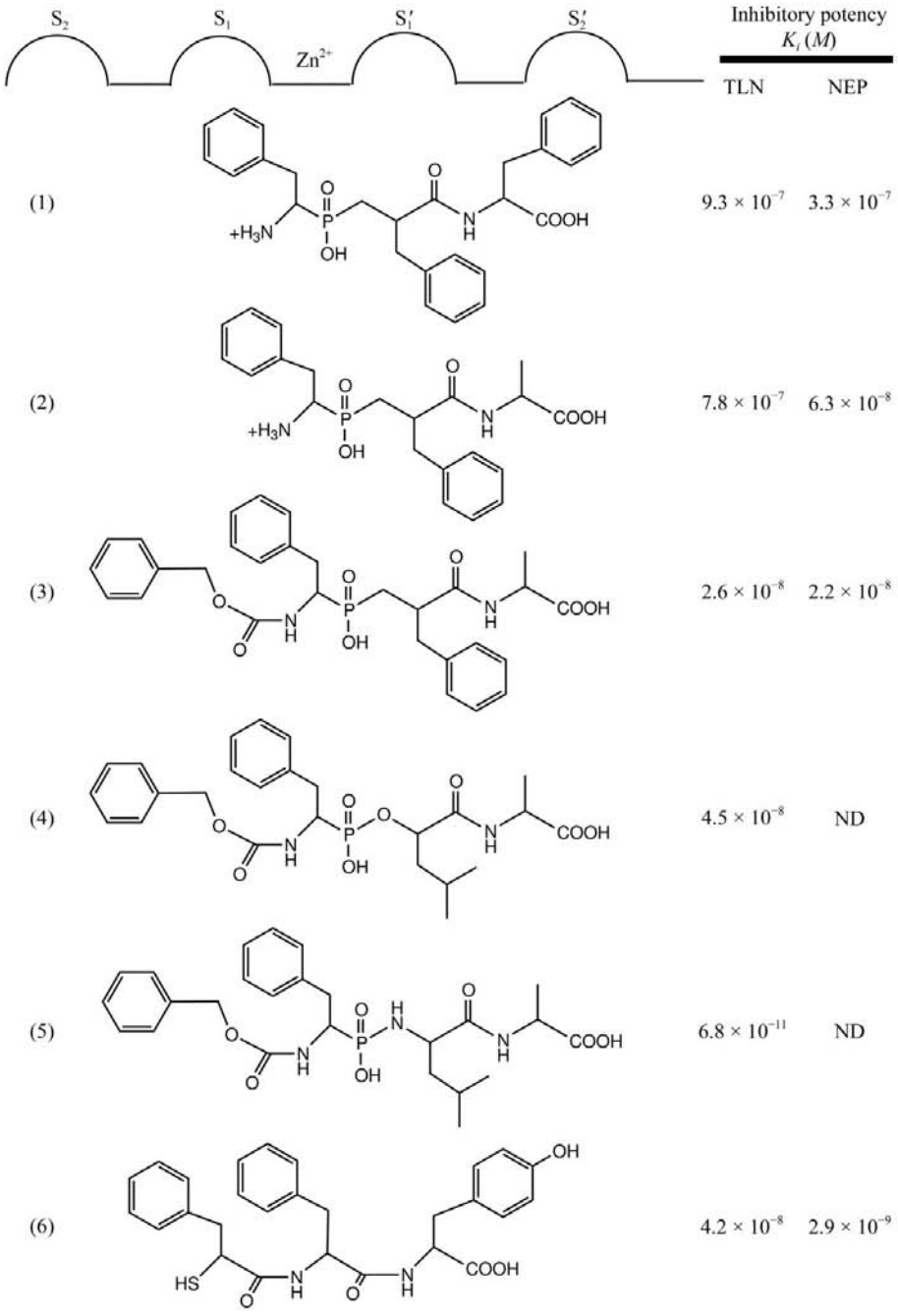

Figure 1
Schematic representation of the four subsites in Zn metallopeptidases according to Schechter & Berger (1967) and the formulae of the six designed inhibitors mentioned in the text, together with their corresponding K_i inhibition constants for TLN and NEP. (1), (2) and (3) are the new phosphinic inhibitors. (1) and (2) differ in the C-terminal peptide (Phe or Ala), while (3) is the *N*-protected derivative of (2). Values for (4) and (5) are from Bartlett & Marlowe (1987) and those for (6) are from Gaucher *et al.* (1999).

It is interesting to observe that the bidentation of zinc results in a significant increase in inhibitory potencies. Until now, the $ZF^{P}LA$ molecule represented the most efficient inhibitor of TLN, with a K_i of $6.7 \times 10^{-11}\,M$ (Bartlett & Marlowe, 1987).

In the search for potent dual inhibitors of both the endopeptidase neprilysin (NEP) and the exopeptidase aminopeptidase N (APN; EC 3.4.11.2) for use as potential analgesics (Chen *et al.*, 1998, 2000), we have developed a number of α-aminophosphinic derivatives with the general formula $^{+}H_3N$-CH(R_1)P(O)(OH)CH_2CH(R'_1)CONH-CH(R'_2)-COOH with R_1, R'_1 and R'_2 suitably designed (Fig. 1). These molecules have low-nanomolar affinities for both NEP and APN enzymes.

To understand these results in terms of endopeptidase *versus* exopeptidase recognition, two questions are addressed. (i) Does the phosphinic group act a monodentate or a bidentate ligand for the zinc as observed in the mercapto inhibitor (6)? (ii) Does the free α-amino group of the inhibitor play a role in NEP recognition?

To answer to these questions, the inhibitor (1) (Fig. 1), which is assumed to recognize the three S_1, S'_1 and S'_2 subsites (Schechter & Berger, 1967) of the enzymes, has been crystallized with TLN as a model for NEP (Tiraboschi *et al.*, 1999; Oefner *et al.*, 2000). As shown in Fig. 1, NEP ($K_i = 3.3 \times 10^{-7}\,M$) and TLN ($K_i = 9.3 \times 10^{-7}\,M$) have similar affinities towards compound (1).

2. Materials and methods

2.1. Chemicals

The inhibitors were synthesized in the laboratory according to Chen *et al.* (2000). Thermolysin was purchased from Sigma (France). Neutral endopeptidase (NEP) was obtained from rabbit kidney and purified to homogeneity as described previously (Aubry *et al.*, 1987).

2.2. Biochemical assays

Inhibitory potencies were determined using (^{3}H)Tyr-Gly-Gly-Phe-Leu (K_M = 2 μ*M*; Benchetrit *et al.*, 1987) as the substrate for TLN and dansyl-D-Ala-(pNO_2)Phe-Gly (K_M = 37 μ*M*) as the substrate for NEP (Goudreau *et al.*, 1994).

Accounting for their competitive nature, the K_i values of inhibitors were determined from their IC_{50} values using the Chen–Prussoff relation [$K_i = IC_{50}/(1 + S/K_M)$] .

2.3. Crystallization

TLN was co-crystallized with inhibitor (1) using the hanging-drop method following previously described procedures (Matthews *et al.*, 1972; Gaucher *et al.*, 1999). Prior to crystallization, added salts were removed from TLN by suspending 13 mg lyophilized TLN in 0.7 ml water followed by centrifugation at 7400*g*. The pellet was dissolved in 100 µl of solution *A* [50 m*M* Tris acetate buffer pH 8.0, 0.5 *M* calcium acetate, 4 m*M* dithiothreitol, 1 m*M* sodium azide and 45%(*v*/*v*) dimethylsulfoxide (DMSO)]. Enzyme concentrations were estimated using an ε_{280} of 56 000 M^{-1} cm^{-1}. 1 µl drops containing TLN (120 mg ml^{-1} or 3.2 m*M* TLN) and 20 m*M* inhibitor (1) in solution *A* were mixed and equilibrated against a 1 ml reservoir containing 520 µl solution *A* and 480 µl water. Hexagonal crystals grew in about one to two months at 278 K.

2.4. Data collections

Diffraction data were recorded at 277 K at the LURE synchrotron facility, Orsay, France. The wavelength was set to 0.962 Å. The crystals were mounted in wet capillaries, usually with the *c* axis misaligned by about 20° with respect to the rotation spindle, in order to minimize loss of data from the 'blind region'. A single crystal was used and 50 frames with a rotation angle of 1° each were collected using a 300 mm diameter MAR Research image-plate system connected to the W32 beamline (Fourme *et al.*, 1992). The crystal-to-detector distance was set to 250 mm. Frames were processed with the *MOSFLM* program (Leslie, 1990) and merged and scaled with *SCALA*; amplitudes were calculated with *TRUNCATE* (Collaborative Computational Project, Number 4, 1994). Table 1 summarizes the results of the data processing.

2.5. Structure solution and refinement

Refinement was carried out by alternate cycles of *CNS* calculation (Brünger *et al.*, 1990) and manual fitting of the model into electron-density maps using *O* (Jones *et al.*, 1991). 10% of the data were used for cross-validation of the refinement (the R_{free} value). A maximum-likelihood target was used in refinements and a bulk-solvent correction with anisotropic *B* factor was applied to low-resolution data.

Table 1
Data-collection and refinement statistics for the TLN–inhibitor (1) complex.

Data collection	
Space group	$P6_122$
Unit-cell parameters (Å)	
$a = b$	93.78
c	132.25
No. of unique reflections	23742
Data redundancy	5.2
All data (19.9–2.0 Å)	
R_{sym} (%)	7.6
Mean $I/\sigma(I)$	16.3
Completeness (%)	91.6
Highest resolution shell (2.1–2.0 Å)	
R_{sym} (%)	12.5
Mean $I/\sigma(I)$	7.4
Completeness (%)	85.5
Refinement (*SHELXL*)	
No. of atoms	
TLN	2432
Inhibitor	35
DMSO, Ca^{2+}, Zn^{2+}	1, 4, 1
Solvent	186
Resolution range (Å)	19.0–2.0
No. of parameters/restraints	10666/10251
R factor (%) for 4σ observed data (No. of data)	13.9 (19094)
R factor (%) for all data (No. of data)	14.6 (21413)
Free R factor (%) for 6% of observed data (No. of data)	17.3 (1903)
R.m.s. deviations (No.)	
1–2 Bond length (Å)	0.021 (2531)
1–3 Bond-distance angles (Å)	0.022 (3447)
Planes (Å)	0.27 (891)
Non-zero chiral volumes (Å^3)	0.049 (364)
Zero chiral volumes (Å^3)	0.028 (401)
Mean isotropic $\langle B \rangle$ values (Å^2)	
Main chain	11.1
Side chain	16.9
Water molecules	31.4
Inhibitor	25.2
Residuals in final Fourier map (min/max) (e$^-$)	–0.25/+0.40

The crystals used in this study were isomorphous to native TLN. The structure of the native TLN solved at room temperature (PDB code 1lnf) was used as the starting model. The complexed dipeptide Val-Lys and all solvent molecules were removed and an overall *B* factor of 16 Å^2 was assigned to all atoms. The refinement began with rigid-body least-squares fitting, followed by refinement of the atomic positions by energy minimization at an initial resolution of 2.5 Å. The resolution was progressively increased to the maximum of 2.0 Å.

The model was subjected to cycles of positional refinement and restrained isotropic atomic temperature-factor refinement. After each cycle of *B*-factor refinement, the model was examined on the graphics system and refitted to the density. Water molecules were added to the model using *WATERPICK* (in *CNS*). They were placed at the positions of large positive (>2σ) peaks in difference Fourier maps provided that they were also present in the $2F_o - F_c$ maps with a suitable hydrogen-bonding environment.

During the course of water localization, electron-density maps clearly showed the position of the ligand (inhibitor) in

the active site (Fig. 2). The phosphonamidate inhibitor ZF^{P}LA (Holden *et al.*, 1987) was used as a template for building a model for the phosphinic inhibitor (1). The model was then fitted to the electron-density map and included in structure-factor calculations during subsequent refinements.

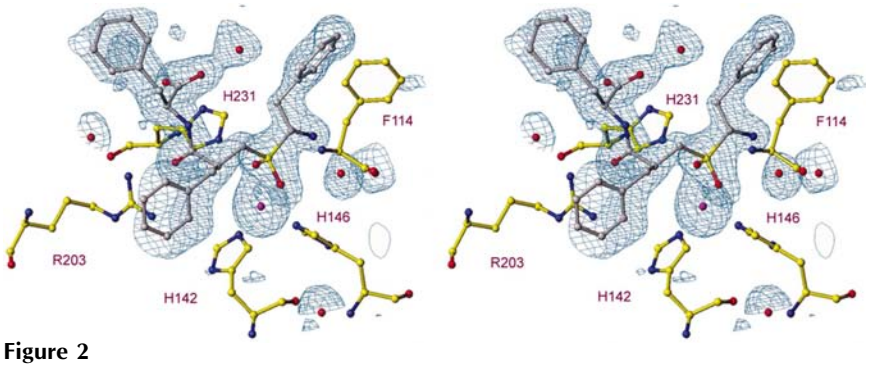

Figure 2
An omit map around the Zn atom calculated at the end of the water-localization steps, before introducing the inhibitor into the structure-factor calculations. The electron density is superimposed on the final refined model of inhibitor (1) (map contouring is 2σ above the mean).

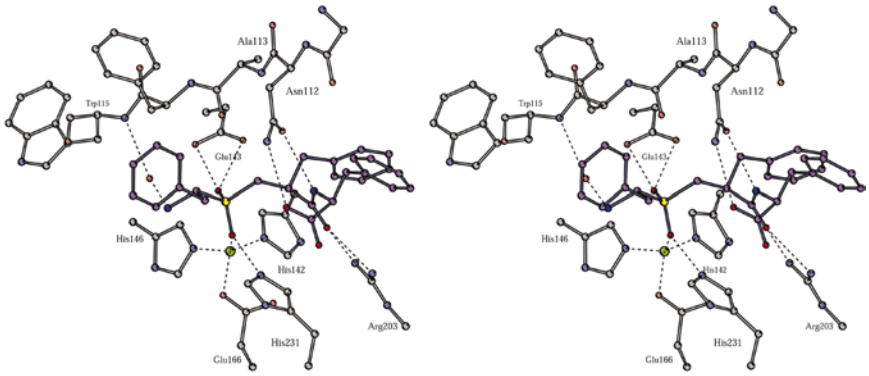

Figure 3
Stereoscopic view of the interactions between the phosphinic inhibitor (1) and TLN in the crystal. Polar bonds are dashed.

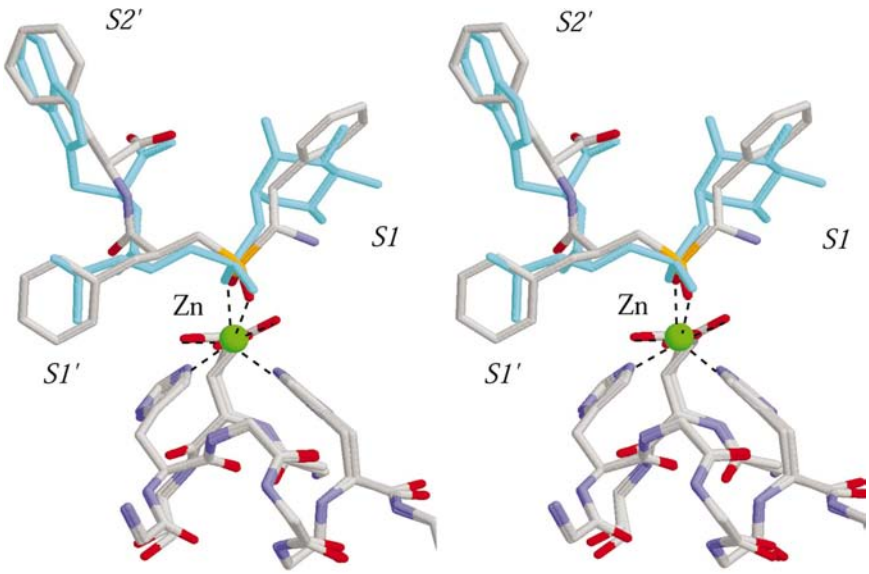

Figure 4
The NEP (Oefner *et al.*, 2000) and TLN active sites superimposed using a *LSQ* fit of their sequences *X*-H-*X*$_3$-H-*X* and *X*-Q-*X* residues, plus the Zn atom. The two inhibitors (1) for TLN and phosphoramidon for NEP (in plain blue) are shown in their bound states: stereoscopic view, *RASMOL* program (Merritt & Bacon, 1997).

In the final stages of the refinement, an important residual electron density which cannot be interpreted as a water molecule because of the absence of putative hydrogen bonding in a hydrophobic environment and because of its broad density shape remained. Although individual atomic positions cannot be distinguished, this density was best modelled as a DMSO molecule. In the last step, the structure was refined against all data (R_{free} = 17.0% before merging the free set) using the *SHELXL* program (Sheldrick & Schneider, 1997). The refinement statistics are given in Table 1.

3. Results

3.1. Quality of the model

The final model consists of 2432 protein atoms, 35 inhibitor atoms, 186 molecules of water and one DMSO moiety plus one zinc and four calcium ions. The structural model is of good quality as indicated by the *PROCHECK* analysis (Laskowski *et al.*, 1993), by the low crystallographic validation statistics (Table 1) and by the small mean deviations of the geometrical parameters from their ideal values. The final *R* factor is 13.9% for the resolution range 10–2.0 Å. The root-mean-square (r.m.s.) coordinate error was estimated to be 0.16 Å from a Luzzati plot (Luzzati, 1952).

3.2. Zinc-binding site

The distances between the zinc ion and the two O atoms of the phosphinic moiety are 1.90 Å (PO1) and 2.90 Å (PO2) (Table 2), indicating that they are both ligands of the zinc, although the coordination of the second oxygen is considerably weaker than that of the first. An equivalent situation was also observed by Tronrud *et al.* (1986) in the TLN–P-Leu-NH$_2$ complex (PO1 = 2.1 Å, PO2 = 2.8 Å). This leads to a structure with a zinc coordination that is intermediate between tetrahedral and a distorted trigonal bipyramid (Table 2). In addition to PO1 and PO2, three residues of TLN are bonded to the zinc ion: His146 NE2, His142 NE2 and Glu166 OE2 (Fig. 3).

3.3. Stabilization of the transition state

In the transition state of the hydrolysis, the carboxyanion formed by water attack on the carbonyl group is expected to be stabilized by various hydrogen bonds

involving either the catalytic Glu143 or His231 or Tyr157 (Matthews, 1988). In the crystal structure of inhibitor (1), the short distances between phosphinic O atoms and these three residues reflect this network of hydrogen bonds: the two O atoms of Glu143 are 2.71 and 2.86 Å from PO2 and the PO1 atom is located 2.88 Å from the imidazole nitrogen NE2 of His231 but at 3.2 Å from the phenolic hydroxyl group of Tyr157.

3.4. Binding subsites

As expected, the three aromatic side chains (R_1, R_1' and R_2') in inhibitor (1) fit the S_1, S_1' and S_2' subsites of the enzyme. The S_1 and S_2' subsites are open and accessible to the solvent and are not well defined. S_1' is a deep hydrophobic cavity which is particularly well suited to the R_1' side chain of the inhibitor. This is illustrated by the low thermal parameters of the R_1' ring (13.3 Å^2) compared with the other aromatic side chains (mean $\langle B \rangle$ factors are 28.2 and 29.3 Å^2 for R_1 and R_2', respectively).

At the N-terminus of the inhibitor, the only interaction that connects this part to the S_1 subsite is the water molecule W470, which forms a bridge between the free amino group of the inhibitor and the amide group of Trp115. Although this water molecule is distant from the Zn atom (4.7 Å), it appears to play a central role as it also stays in the vicinity of O2P of the inhibitor (d = 2.91 Å) and Glu143 O1E (d = 3.0 Å). R_1 (the phenyl ring) is essentially free. At the same time, the R_1' and R_2' side chains are stabilized by a set of hydrogen bonds within their respective subsites: the carbonyl oxygen of R_1' is hydrogen bonded to both the NH1 atom (2.69 Å) and the NH2 atom (2.91 Å) of Arg203, while the Phe moiety of the inhibitor (the C-terminus) interacts through two weak hydrogen bonds with Asn112: d(Phe NH–Asn112 OD1) = 3.19 Å and d(Phe O–Asn112 ND2) = 3.09 Å. The carboxylate group of the inhibitor is also bound to two water molecules (W493 and W586).

4. Discussion

The three-dimensional structure of the TLN–compound (1) complex obtained in this study shows that the essential interactions stabilizing an inhibitor in the active site of this enzyme are satisfied, at least at the level of the catalytic site and its 'prime' domain. In contrast, recognition of the S_1 subsite ('non-prime' domain) by the N-terminal benzylic moiety of inhibitor (1) is less important as expected.

It has previously been shown by crystallization of the phosphonamidate inhibitor ZF^{P}LA (Holden *et al.*, 1987) with TLN that the backbone of the inhibitor binds *via* hydrogen bonds to the protein backbone of Trp115 as an antiparallel β-sheet. In this complex, the carbonyl oxygen of the benzyloxycarbonyl (Cbz) moiety of the inhibitor makes an efficient hydrogen bond (2.9 Å) with the amide nitrogen of Trp115.

In the present complex with inhibitor (1), there is no enzyme–inhibitor interaction involving a Cbz moiety, but the free α-amino group of (1) is hydrogen bonded *via* a water molecule to Trp115 NH in a similar way to the amide nitrogen of Gly in ZG^{P}LA ($K_i = 1.6 \times 10^{-8}$ M; Holden *et al.*, 1987). The co-crystallization of (1) and TLN was achieved at pH 8, supporting the presence of an unprotonated form of the free amino group.

Table 2
Geometry around Zn^{2+} in the inhibitor (1)–TLN complex.

Angles (°).

His142 NE2—Zn—Inh O1P	114.2
His146 NE2—Zn—Inh O1P	125.1
Glu166 OE2—Zn—Inh O1P	95.0
His142 NE2—Zn—Inh O2P	91.2
His146 NE2—Zn—Inh O2P	85.1
Glu166 OE2—Zn—Inh O2P	140.8

Distances (Å).

Zn—His142 NE2	2.03
Zn—His146 NE2	2.02
Zn—Glu166 OE2	1.94
Zn—Inh O1P	1.90
Zn—Inh O2P	2.90

The mode of recognition of the TLN active site by compound (1) is very similar to that described recently for compound (6) (Gaucher *et al.*, 1999). Indeed, both compounds (i) occupy an extended domain encompassing the S_1–S_2' subsites, (ii) act as bidentate ligands of the catalytic Zn ion and (iii) satisfy the set of hydrogen bonds involving Arg203 and Asn112 as commonly found in TLN–inhibitor complexes (Matthews, 1988). Therefore, similar inhibitory potencies might be expected for both inhibitors. However, the phosphonic inhibitor (1) ($K_i = 9.3 \times 10^{-7}$ M) is 50-fold less efficient than compound (6) ($K_i = 2 \times 10^{-8}$ M) towards TLN. Several explanations could be proposed to account for this apparent discrepancy.

Firstly, there is no donor group in compound (1) that interacts with the carbonyl of Ala113, as observed in the complex of TLN with (6) (Gaucher *et al.*, 1999). This interaction is very important in terms of the affinity constant as deduced from comparison between the K_i values of ZF^{P}LA (5) ($K_i = 6.8 \times 10^{-11}$ M) and ZF^P(O)LA (4) ($K_i = 4.5 \times 10^{-8}$ M) towards TLN (Bartlett & Marlowe, 1987).

Secondly, differences in solvation of the free and bound inhibitors (1) and (6) could also account for their respective inhibitory potencies. Furthermore, the presence of a CH_2 group in the vicinity of the zinc-chelating phosphonic moiety provides a larger flexibility in (1) compared with (6) in solution. This could introduce an unfavourable entropic factor during the enzyme-recognition process in the case of (1). It is interesting to note that no head-to-tail hydrogen bonding was observed by NMR (not shown) for compound (1) in solution.

It cannot be excluded that the strength of zinc coordination by the thiol and oxygen groups in (6) is higher than the bidentate interaction of the phosphonic group in (1). This seems to be supported by the similarity in the K_i values of (6) and (4), despite there being no binding to the S_2 subsite in (6).

TLN is currently taken as a model for zinc-metalloendopeptidases such as NEP, thus assuming a great similarity in the

mechanism of action and active-site structures. This has been recently confirmed by computer modelling (Tiraboschi *et al.*, 1999) and crystallographic analysis (Oefner *et al.*, 2000).

A comparison of TLN and NEP inhibition is given in Fig. 4. The two active sites are superimposed with the Zn atom as a pivot and showing the two coordinated histidines (His142 and His146 for TLN; His583 and His587 for NEP) and the glutamic acid (Glu166 for TLN; Glu646 for NEP). The two inhibitors (1) (for TLN) and phosphoramidon (for NEP) are shown according to the *LSQ* fits of their active sites. Although they show similar backbone conformations, orientations and coordination around the Zn atom, they display some differences as observed in the S_1 and S_2' subsites. Two immediate observations can be made: (i) the rhamnose moiety in the NEP–phosphoramidon structure only makes a weak polar interaction through the ring oxygen (none of the hydroxyls O2, O3 or O4 are involved in interactions) and (ii) in the S_2' subsite the aromatic ring moiety adopts a different stacking orientation.

Using these data, we need to explain why the protection of the free α-amino group of (2) with a Cbz group in (3) only induces a threefold change in the K_i value for NEP, but a 50-fold change for TLN. This result could be interpreted as a difference in the S_1–S_2 domains of NEP compared with TLN. In the latter enzyme, the S2 subsite is significantly hydrophobic, as illustrated by the high potency of inhibitors wrapping the four S_2, S_1, S_1' and S_2' subsites with lipophilic side chains (compound 5).

In the case of NEP, as previously outlined, inhibition is essentially ensured by the S_1' and S_2' subsite occupancy: hence, thiorphan and its analogues (Roques *et al.*, 1980; Fournié-Zaluski *et al.*, 1984) inhibit NEP in the nanomolar range. Compounds containing side chains that are potentially able to recognize the S_1–S_2 domains are less efficient with regard to NEP inhibition (Mumford *et al.*, 1982; Chen *et al.*, 2000) and polar groups, such as the free amino group in (1), have no effect. This seems to indicate that the putative S_1–S_2 domain in NEP is freely accessible to the solvent and that there are no stabilizing interactions involving this part of the active site. This finding is supported by the large solvent accessibility of rhamnose moiety in the recently published crystalline structure of the phosphoramidon–NEP complex (Oefner *et al.*, 2000).

References

Aubry, M., Bertheloot, A., Beaumont, A., Roques, B. P. & Crine, P. (1987). *Biochem. Cell Biol.* **65**, 398–404.

Bartlett, P. A. & Marlowe, C. K. (1983). *Biochemistry*, **22**, 4618–4624.

Bartlett, P. A. & Marlowe, C. K. (1987). *Biochemistry*, **26**, 8553–8561.

Benchetrit, T., Fournié-Zaluski, M. C. & Roques, B. P. (1987). *Biochem. Biophys. Res. Commun.* **147**, 1034–1040.

Bode, W., Gomis-Rüth, F. X. & Stöckler, W. (1993). *FEBS Lett.* **331**, 134–140.

Bohacek, R., De Lombaert, S., McMartin, C., Priestle, J. & Grütter, M. (1996). *J. Am. Chem. Soc.* **118**, 8231–8249.

Brünger, A. T., Krukowski, A. & Erickson, J. W. (1990). *Acta Cryst.* A**46**, 585–593.

Chen, H., Noble, F., Coric, P., Fournié-Zaluski, M. C. & Roques, B. P. (1998). *Proc. Natl Acad. Sci. USA*, **95**, 12028–12033.

Chen, H., Noble, F., Mothé, A., Meudal, H., Coric, P., Danascimento, S., Roques, B. P., George, P. & Fournié-Zaluski, M. C. (2000). *J. Med. Chem.* **43**, 1398–1408.

Collaborative Computational Project, Number 4 (1994). *Acta Cryst.* D**50**, 760–764.

Fourme, R., Dhez, P., Benoit, J. P., Kahn, R., Dubuisson, J. M., Besson, P. & Frouin, J. (1992). *Rev. Sci. Instrum.* **63**, 982–987.

Fournié-Zaluski, M. C., Soroca-Lucas, E., Waksman, G. & Roques, B. P. (1984). *Eur. J. Biochem.* **139**, 267–274.

Gaucher, J. F., Selkti, M., Tiraboschi, G., Prangé, T., Roques, B. P., Tomas, A. & Fournié-Zaluski, M. C. (1999). *Biochemistry*, **38**, 12569–12576.

Goudreau, N., Guis, C., Soleilhac, J. M. & Roques, B. P. (1994). *Anal. Biochem.* **219**, 87–95.

Hangauer, D. G., Monzingo, A. F. & Matthews, B. W. (1984). *Biochemistry*, **23**, 5730–5741.

Hanson, M. A. & Stevens, R. C. (2000). *Nature Struct. Biol.* **7**, 687–692.

Holden, H. M., Tronrud, D. E., Monzingo, A. F., Weaver, L. H. & Matthews, B. W. (1987). *Biochemistry*, **26**, 8542–8553.

Jones, T. A., Zou, J. Y., Cowan, S. W. & Kjeldgaard, M. (1991). *Acta Cryst.* A**47**, 110–119.

Kam, C. M., Nishino, N. & Powers, J. C. (1979). *Biochemistry*, **18**, 3032–3038.

Komiyama, T., Suda, H., Aoyagi, T., Takeuchi, T., Umezawa, H., Fujimoto, K. & Umezawa, S. (1975). *Arch. Biochem. Biophys.* **171**, 727–731.

Laskowski, R. A., MacArthur, M. W., Moss, D. S. & Thornton, J. M. (1993). *J. Appl. Cryst.* **26**, 283–291.

Leslie, A. G. W. (1990). *Crystallographic Computing 5: From Chemistry to Biology*, edited by D. Moras, A. D. Podjarny & J. C. Thierry, pp. 60–61. Oxford University Press.

Luzzati, V. (1952). *Acta Cryst.* **5**, 802–810.

Matthews, B. W. (1988). *Acc. Chem. Res.* **21**, 333–340.

Matthews, B. W., Jansonius, J. N., Colman, P. M., Shoenborn, B. & Dupourque, D. (1972). *Nature New Biol.* **238**, 37–41.

Merritt, E. A. & Bacon, D. J. (1997). *Methods Enzymol.* **277**, 505–524.

Mumford, R. A., Zimmerman, M., ten Broeke, J., Taub, D., Joshua, H., Rothrock, J. W., Hirshfield, J. M., Springer, J. P. & Patchett, A. A. (1982). *Biochem. Biophys. Res. Commun.* **109**, 1303–1309.

Natesh, R., Schwager, S. L., Sturrock, E. D. & Acharya, K. R. (2003). *Nature (London)*, **421**, 551–554.

Oefner, C., D'Arcy, A., Hennig, M., Winkler, F. K. & Dale, G. E. (2000). *J. Mol. Biol.* **296**, 341–349.

Roques, B. P., Fournié-Zaluski, M. C., Soroca, E., Lecomte, J. M., Malfroy, B., Llorens, C. & Schwartz, J. C. (1980). *Nature (London)*, **288**, 286–288.

Sansom, C. E., Hoang, M. V. & Turner, A. J. (1998). *Protein Eng.* **11**, 1235–1241.

Schechter, I. & Berger, A. (1967). *Biochem. Biophys. Res. Commun.* **27**, 157–162.

Sheldrick, G. M. & Schneider, T. R. (1997). *Methods Enzymol.* **277**, 319–343.

Swaminathan, S. & Eswaramoorthy, S. (2000). *Nature Struct. Biol.* **7**, 693–699.

Thunnissen, M. M., Nordlund, P. & Haeggström, J. Z. (2001). *Nature Struct. Biol.* **8**, 131–135.

Tiraboschi, G., Jullian, N., Théry, V., Antonczak, S., Fournié-Zaluski, M. C. & Roques, B. P. (1999). *Protein Eng.* **12**, 141–149.

Tronrud, D. E., Holden, H. M. & Matthews, B. W. (1987). *Science*, **235**, 571–574.

Tronrud, D. E., Monzingo, A. F. & Matthews, B. W. (1986). *Eur. J. Biochem.* **157**, 261–268.

Umezawa, S., Tatsuta, K., Izawa, O. & Tsuchiya, T. (1972). *Tetrahedron Lett.* **1**, 97–100.

Weaver, L. H., Kester, W. R. & Matthews, B. W. (1977). *J. Mol. Biol.* **114**, 119–132.